Numerical Analysis of a Tunnel in Residual Soils

Roberto F. Azevedo[1]; Alexandre B. Parreira[2]; and Jorge G. Zornberg, M.ASCE[3]

Abstract: This paper presents results of an elastoplastic finite element back analysis of a shallow tunnel through residual soils. The tunnel was constructed as part of the expansion of the underground transit system in the city of São Paulo, Brazil. A comprehensive laboratory testing program on undisturbed soil samples was performed in order to characterize the stress–strain–strength behavior of the residual soils. Results from this laboratory testing program were used to calibrate a nonassociated elastoplastic constitutive model utilized to reproduce the behavior of the residual soils under stress paths typical of underground excavation. A stress transfer method is proposed to simulate, using a two-dimensional finite element analysis, the response of the soil mass to the three-dimensional advancement of a tunnel excavation. Comparisons are presented between monitored displacements from an instrumented section of the Paraíso tunnel, empirical predictions, and the results of a finite element back analysis. Good agreement is achieved between the displacements obtained from field instrumentation data and the empirical and numerical results.

DOI: 10.1061/(ASCE)1090-0241(2002)128:3(227)

CE Database keywords: Numerical analysis; Residual soils; Tunnels; Finite elements; Constitutive models; Excavation; Overconsolidated clays.

Introduction

New underground transportation systems have been constructed and significant upgrades to existing infrastructures took place within the last decade in major cities in Brazil. In particular, the subway system in São Paulo, the largest city in South America, underwent a recent major expansion. Part of the subway construction was performed using cut-and-cover excavation procedures. However, as the subway served the populous São Paulo financial district, most of its expansion was constructed using shallow tunneling techniques for excavating the typical residual soils of the São Paulo basin.

Prediction of ground movements within the soil mass surrounding excavations is a major design issue, particularly in densely populated urban areas. Numerical modeling (e.g., the finite element method) has been used for evaluation of the behavior of excavation projects in big metropolises. However, the accuracy of the numerical modeling effort depends to a large extent on the adequacy of the stress–strain–strength relationships used to represent the behavior of the soils surrounding the excavation. Specifically, the constitutive model should be able to capture the soil behavior under stress paths typical in excavation projects.

Elastoplastic models have been particularly useful in representing the behavior of soils. However, most of the reported experience has been on the use of these models with reconstituted clays and sands. So far, little experience has been accumulated on the use of elastoplastic models to represent the behavior of geotechnical structures involving undisturbed, unsaturated soils. This seems to be also the case of tunneling through residual soils (Negro 1998).

Prediction of ground displacements induced by shallow underground excavations also requires adequate simulation of the sequential construction stages. Two-dimensional (2D) finite element analyses have been performed to simulate excavations, particularly when construction involves open-cut procedures (e.g., Whittle et al. 1993; Zornberg and Azevedo 1998). When construction involves tunnel excavation, the numerical simulation would ideally be performed using three-dimensional (3D) analyses (Augarde et al. 1994; Walter 1997; Targas et al. 1998). However, 3D analyses of geotechnical projects involving the use of nonlinear solvers to handle elastoplastic soil models are normally not performed due to high computational costs. Thus, methods that account for 3D effects using 2D approximate analysis have been proposed (Panet and Guenot 1982; Schikora and Ostermeier 1988; Bernat and Cambou 1995; Malato et al. 1998). These simplified methods are generally based on approaches such as ''stiffness softening'' and ''stress relaxation''. The first approach involves a progressive decrease of the stiffness of the excavated elements along with the progressive application of boundary stresses. The stress relaxation approach involves the complete removal of the excavated elements stiffness before the boundary stresses are progressively applied. None of these approaches, however, allows for proper simulation of the construction of the tunnel lining system (Negro and Eisenstein 1991).

In this paper, a comprehensive laboratory testing program is described which includes testing of undisturbed samples of residual soils sheared under stress paths representative of excavations. The results of this experimental program were utilized to calibrate the nonassociated elastoplastic model (Lade 1977, 1979) used to represent the behavior of the residual soils. A stress transfer method is then proposed to simulate, using a 2D elasto-plastic

[1]Professor, Federal Univ. of Viçosa, Viçosa, Minas Gerais, Brazil. E-mail: razevedo@mail:ufv.br

[2]Assistant Professor, Univ. of São Paulo, São Carlos, São Paulo, Brazil.

[3]Assistant Professor, Univ. of Colorado at Boulder, Boulder, CO 80309.

Note. Discussion open until August 1, 2002. Separate discussions must be submitted for individual papers. To extend the closing date by one month, a written request must be filed with the ASCE Managing Editor. The manuscript for this paper was submitted for review and possible publication on June 14, 1999; approved on May 29, 2001. This paper is part of the ***Journal of Geotechnical and Geoenvironmental Engineering***, Vol. 128, No. 3, March 1, 2002. ©ASCE, ISSN 1090-0241/2002/3-227–236/$8.00+$.50 per page.

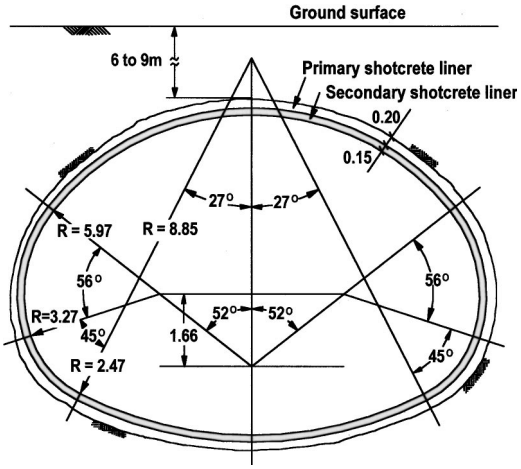

Fig. 1. Tunnel cross section (lengths in meters)

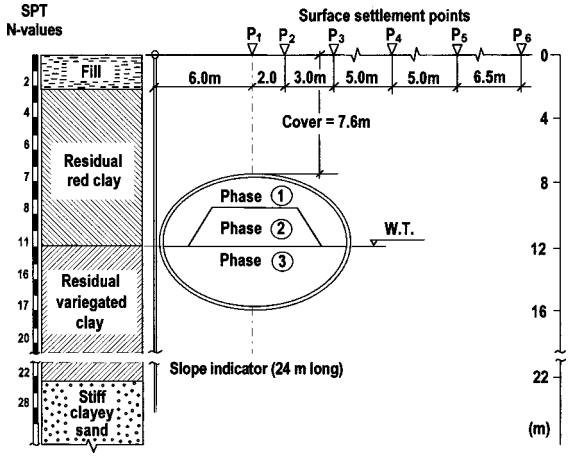

Fig. 2. Geotechnical profile, tunnel construction phases, and instrumentation

finite element analysis implemented in the code *ANLOG* (Zornberg and Azevedo 1990), the 3D characteristics of a tunnel advancement. Comparisons are presented between numerical results obtained after the tunnel construction, empirical predictions, and field instrumentation data.

Project Description and Subsurface Conditions

The tunnel analyzed in this study was part of the expansion of the underground transit system in São Paulo, Brazil. The tunnel section evaluated in this paper is part of the Paulista line, a 4.5 km long portion of the expansion completed in 1991, which serves an important financial district of the city. Because of the major traffic problems that an open-cut excavation would have imposed on the region, a tunnel excavation approach was selected. The tunnel was constructed using either a tunneling boring machine method or a sequential excavation method (Eisenstein and Sorensen 1986).

The section of the Paulista line evaluated in this paper, the Paraíso tunnel, is located near the Paraíso station and was built using a sequential excavation method. The tunnel, approximately 103 m long, has a maximum height of 8.4 m and a maximum width of 11.4 m (82 m^2 net area). Fig. 1 shows a cross section of the tunnel. The thickness of the soil cover above the tunnel crown ranges from 6 to 9 m. Specifically, the soil cover thickness at the instrumented section analyzed in this paper is 7.6 m. The support system consists of a 0.20 m-thick primary shotcrete and a 0.15 m-thick secondary shotcrete liner.

The Paraíso tunnel was excavated through residual soils of the São Paulo basin, a tertiary sedimentary deposit of fluvial-lacustrine origin. The sediments in the São Paulo basin underwent a weathering process that left characteristics such as mottling and precompression caused by desiccation. Massad et al. (1985) and Kupper et al. (1985) investigated the geotechnical characteristics of the residual soils of the São Paulo basin. A typical geotechnical profile includes an upper layer of ''residual red clay'' underlain by a layer of ''residual variegated clay''. The residual red clay is normally located above the water table and typically shows two horizons, with the upper one generally showing more intense weathering. The structure of the residual red clay is notoriously open, with a void ratio often exceeding 1.0.

The geotechnical profile at the location of the Paraíso tunnel is shown in Fig. 2. Fill material constitutes the upper 2 m of the profile and is underlain by an approximately 9 m thick layer of residual red clay. This residual soil is a porous and slightly overconsolidated [overconsolidation ratio (OCR) 2 to 3] clay with standard penetration test (SPT) blow counts ranging from 4 to 11. The layer of residual variegated clay is approximately 11 m thick at this location. This soil is a stiff, fissured, overconsolidated (OCR 5 to 6) clay with SPT blow counts ranging from 16 to 22. These residual clay materials underwent a laterization process after their deposition in the tertiary age. A very stiff clay sand layer with a SPT blow count ranging from 28 to 35 underlies the residual clay layers. The groundwater table is located at a depth of 12 m, approximately between the residual red clay and the residual variegated clay layers. As indicated in Fig. 2, the upper and lower halves of the tunnel were excavated, respectively, through the residual red clay and the residual variegated clay layers.

A slope indicator and six surface settlements points were installed at a transversal section of the Paraíso tunnel to monitor displacements of the adjacent soil mass. Location of these instruments is also shown in Fig. 2. Fig. 2 also illustrates the construction sequence of the Paraíso tunnel, which included three phases. The first phase, excavation of the tunnel crown, was performed in 1.6 m long segments. Primary support consisted of I-shaped 127 mm height steel ribs, and 0.20 m thick shotcrete liner. After the installation of this support system, the central ground core was excavated (Phase 2 in Fig. 2). These two phases were repeated until a maximum heading advance of 7 m. Finally, the bench was excavated in 1.6 m long segments (Phase 3 in Fig. 2). A primary support system similar to that used in the heading excavation was used, but without any invert support structure. After completion of the tunnel excavation, the thickness of the shotcrete liner was increased to 0.35 m.

Behavior of São Paulo Residual Soils

Laboratory Testing Program

A comprehensive laboratory testing program using undisturbed samples of the residual soils was undertaken as part of this investigation in order to characterize the stress–strain–strength behavior of the residual soils in the São Paulo sedimentary deposit (Parreira 1991). Results of this testing program were subsequently used to calibrate the elastoplastic model employed in the numerical analyses described herein.

Table 1. Soil Properties

Property	Residual red clay (3.5 m)	Residual red clay (6.5 m)	Residual variegated clay (9.5 m)	Residual variegated clay (12.5 m)
W(%)	41.5	41.0	36.5	37.1
e	1.62	1.52	1.04	1.02
Sr(%)	69.6	72.4	92.2	96.8
γ_{nat}(kN/m^3)	14.4	14.7	17.2	17.8
Gs	2.72	2.68	2.63	2.65
LL	78.8	73.8	89.5	90.8
IP	29.3	25.7	42.1	43.4
σ_{pc}(kPa)	127.5	196.0	760.0	814.0

Undisturbed soil block samples (50 cm long sides) were collected in a test pit located close to the Paraíso tunnel. Blocks of residual red clay were collected at depths of 3.5 and 6.5 m, and blocks of residual variegated clay were collected at depths of 9.5 and 12.5 m. Table 1 shows in situ moisture content, w, void ratio, e, degree of saturation, S_r, in situ unit weight, γ_{nat}, specific gravity of soil solids, Gs, liquid limit, LL, plasticity index, PI, and the overconsolidation pressure, σ_{pc}, of the residual soils. Both soils show a comparatively high in situ void ratio.

Considering that the behavior of the residual red clay was very sensitive to moisture variations because of its open structure, laboratory testing of this material was performed using soil specimens at the in situ moisture content. Laboratory testing of the residual variegated clay was performed using back-pressure saturated specimens.

Conventional laboratory tests are generally performed following compression loading stress paths. However, in situ stresses within the soil mass surrounding tunnel excavations generally follow vertical and horizontal unloading stress paths (Ng and Lo 1985). To adequately stimulate the field behavior, the laboratory testing program included isotropically consolidated drained triaxial tests, under both loading and unloading stress paths. Specifically, the testing program performed for the investigation included hydrostatic compression tests (HC), conventional triaxial compression tests (CTC), reduced triaxial compression tests (RTC), and reduced triaxial extension tests (RTE). The stress paths used in the testing program are illustrated in Fig. 3.

The CTC and RTE tests were performed using a strain-controlled triaxial cell loading device, whereas the RTC tests were conducted using a stress-controlled triaxial cell loading device. Radial displacements were measured directly on the soil specimens during the tests using a C-shaped aluminum clamp instrumented with strain-gages (Parreira 1991).

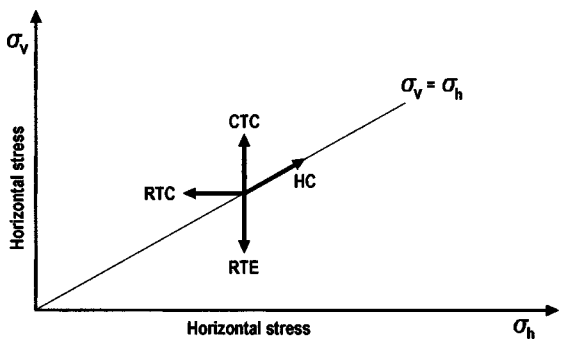

Fig. 3. Stress paths used in testing program

Characteristics of Constitutive Model

The elastoplastic model developed by Lade (1977, 1979) was used to represent the stress–strain–strength behavior of the residual soils. This model has been used to characterize the behavior of remolded soils (either sands or normally consolidated clays) under saturated and dry conditions.

A brief overview of the original model and additional features used in this investigation are presented herein in order to define relationships and parameters used later in the paper. The elastoplastic model uses an isotropic work-hardening framework and considers two yield surfaces: a conical-shaped yield surface characterized by a nonassociated flow rule (plastic expansive surface), and a cap-type yield surface governed by an associated flow rule (plastic collapsive surface). Accordingly, the total strain increments are divided into elastic, plastic expansive, and plastic collapsive components.

The elastic strain increments are calculated using Hooke's law assuming a constant Poisson's ratio, ν, and a Young's modulus, E, given by

$$E = K_{ur} p_a (\sigma_3 / p_a)^n \tag{1}$$

where p_a = atmospheric pressure; K_{ur} and n = model parameters; and σ_3 = minor principal effective stress.

The plastic collapsive strain increments are calculated using an associated flow rule and a yield function F_c, which is a function of the effective stress tensor, σ, and of the plastic collapsive work, W_c. The plastic yield function F_c is given by

$$F_c(\sigma, W_c) = f_c(\sigma) - (p_a/p)^2 (W_c/p_a - c)^2 = 0 \tag{2}$$

where c and p = model parameters and f_c = collapsive stress level defined as

$$f_c(\sigma) = I_1^2 + 2I_2 \tag{3}$$

where I_1 and I_2 = first and second stress invariants ($I_1 = \sigma_1 + \sigma_2 + \sigma_3$, $I_2 = -\sigma_1\sigma_2 - \sigma_1\sigma_3 - \sigma_2\sigma_3$) and σ_1 and σ_2 = major and intermediate principal effective stresses.

Plastic expansive strain increments are calculated using a nonassociated flow rule. The yield function F_p is a function of the effective stress tensor, σ, and of the plastic expansive work, W_p. The expansive yield function F_p is given by

$$F_p(\sigma, W_p) = f_p(\sigma) - a e^{-bW_p} (W_p/p_a)^{1/q} \tag{4}$$

where a, q, and b vary with the confining pressure and f_p = expansive stress level defined as:

$$f_p(\sigma) = (I_1^3/I_3 - 27)(I_1/p_a)^m \tag{5}$$

where I_3 = third stress invariant ($I_3 = \sigma_1\sigma_2\sigma_3$) and m = a model parameter. The constants a, b, and q are related to the confining pressure by additional four model parameters (ψ, Γ, P, and l).

The plastic potential function, g_p, used to define the expansive plastic strains is:

$$g_p = I_1^3 - [27 + \eta_2 (p_a/I_1)^m] I_3 \tag{6}$$

where η_2 is defined as

$$\eta_2 = S f_p + R(\sigma_3/p_a)^{1/2} + t \tag{7}$$

and S, t, and R = model parameters.

Failure is defined when the expansive stress level $f_p(\sigma)$ satisfies the condition:

$$f_p = \eta_1 \tag{8}$$

where η_1 = model parameter. A mobilized shear strength is defined for the purposes of this investigation as the SR given by

$$SR = \eta_1 / f_p \quad (9)$$

$SR = 1$ when the soil reaches its maximum shear strength and tends toward infinity when the soil approaches a hydrostatic compression condition.

Lade's original model requires 14 parameters: three of them define the elastic strain increment (K_{ur}, n, and ν); two parameters define the plastic collapsive strain increment (p and c); two of them define failure (η_1 and m); three parameters define the direction of the plastic expansive strain increment (S, R, and t); and four of them define the magnitude of the plastic expansive strain increment (ψ, Γ, p, and l). All these parameters can be obtained from HC and CTC drained tests with volume change measurements.

The residual red clay is unsaturated at the Paraíso tunnel site. Suction in an unsaturated soil influences the deformability and shear strength of the material (Alonso et al. 1990; Leroueil 1997). In order to approximately account for the unsaturated condition of the residual red clay, the laboratory tests were performed using specimens at the in situ moisture content. For this soil, Lade's model parameters obtained with these tests were used to analyze the field condition assuming that only small changes of moisture content occur in the field and that these small changes do not cause significant variation in suction.

The residual red clay and the residual variegated clay are overconsolidated soils. In order to account for the overconsolidated condition of the soil when using Lade's model, a procedure was implemented to determine the initial location of the yield functions f_{p0} and f_{c0}. Unlike for normally consolidated soils, stress levels f_{p0} and f_{c0} do not correspond to the stress levels f_p and f_c defined by the in situ stresses within the soil mass. Instead, the determination of f_{p0} and f_{c0} is made using Eqs. (3) and (5), respectively; assuming that σ_1 equals the preconsolidation pressure obtained from oedometer testing and $\sigma_3 = \sigma_1 \cdot K_0$, where K_0 is the at-rest earth pressure coefficient.

A slight modification was also incorporated to the original elastoplastic model to better fit the residual soils experimental data. The model parameter S, used in the original formulation to define the relationship between the plastic potential parameter η_2 and the expansive stress level f_p was defined as a function of the confining pressure as follows:

$$S = s_1 + s_2(\sigma_3 / p_a)^{1/2} \quad (10)$$

where s_1 and s_2 = model parameters. With this modification, a total of 15 parameters would be required to model the behavior of the residual soils.

Comparisons between Laboratory Results and Model Predictions

The calibration procedure to obtain the elastoplastic parameters is described by Lade (1977, 1979) and will not be repeated here. The elastic parameters were obtained from unloading–reloading cycles; the plastic collapsive parameters were obtained from HC tests results, and the failure and plastic expansive parameters were obtained from CTC tests results (Parreira 1991). Table 2 presents the nondimensional parameters obtained using the calibration procedure suggested by Lade (1977, 1979). The parameters were obtained for the residual red clay using results from samples collected at depths of 3.5 and 6.5 m. Since residual variegated clay at depths of 9.5 and 12.5 m showed similar behavior, results from these depths were combined in the analysis.

Table 2 also shows the stress levels f_{c0} and f_{p0}, which define the initial location of the collapsive and expansive yield surfaces for the overconsolidated residual clays. These stress levels were defined using an overconsolidation pressure of 760 kPa and a coefficient K_0 of 0.84 for the residual variegated clay. An overconsolidation pressure of 127.5 kPa and K_0 of 0.58 were used for the residual red clay at a depth representative of 3.5 m. The residual red clay at a depth of 6.5 m was normally consolidated and, consequently, f_{p0} was assumed equal to zero.

Table 2. Lade's Model Soil Parameters

Parameter	Residual red clay (3.5 m)	Residual red clay (6.5 m)	Residual variegated clay (9.5 and 12.5 m)
K_{ur}	98.50	153.97	1526
n	−0.15	0.57	0.61
ν	0.27	0.27	0.17
c	...	...	...
p	0.0387	0.0199	0.00408
η_1	138.40	133.63	254.80
m	1.24	0.88	0.992
s_1	0.30	0.41	1.35
s_2	0.19	0.00	−0.16
R	31.39	3.68	−253.64
t	−58.72	−17.47	45.23
P	0.400	0.414	0.043
l	0.370	0.446	1.883
ψ	0.90	1.65	6.11
Γ	0	0	−0.7
fc_0 (kPa^2)	27,193	0	1,392,709
fp_0	10.23	0	5.49

Note: All parameters are dimensionless, unless stated otherwise.

The parameters listed in Table 2 were used to represent the behavior of the residual red clay and residual variegated clay under HC, CTC, RTC, and RTE stress paths. Fig. 4 shows a very good agreement between experimental results under a HC stress path and the behavior predicted by Lade's model. Figs. 5 and 6 compare model predictions with experimental results obtained for the residual red clay and the residual variegated clay under a CTC stress path. The agreement is good for both the deviatoric stress and the volumetric strain curves.

Fig. 7 compares the behavior of residual red clay from RTC tests as predicted by Lade's model and as obtained from the labo-

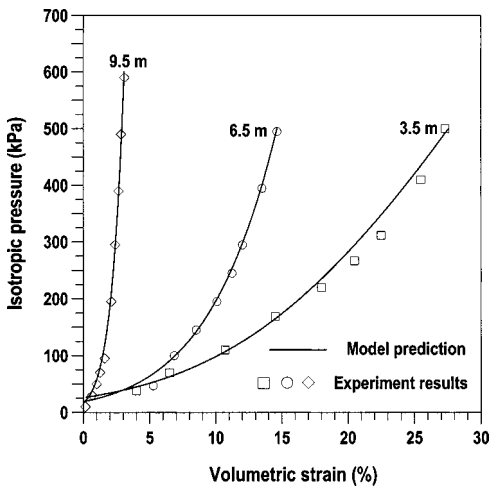

Fig. 4. Hydrostatic compression test results and model predictions

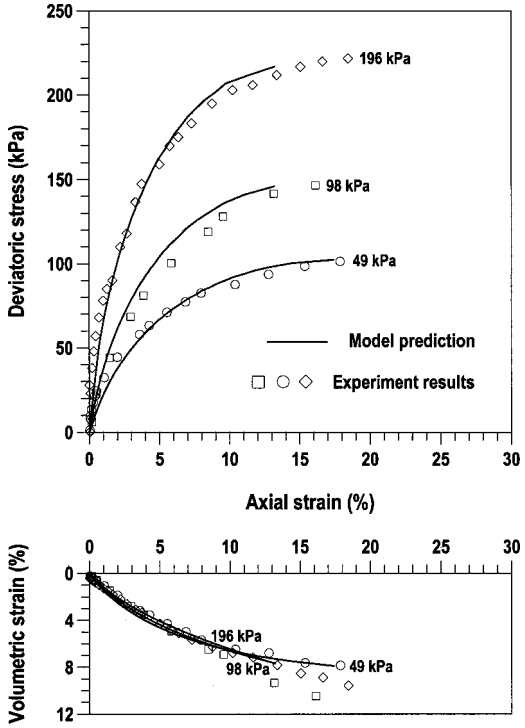

Fig. 5. Conventional triaxial compression test results and model predictions. Residual red clay (6.5 m deep).

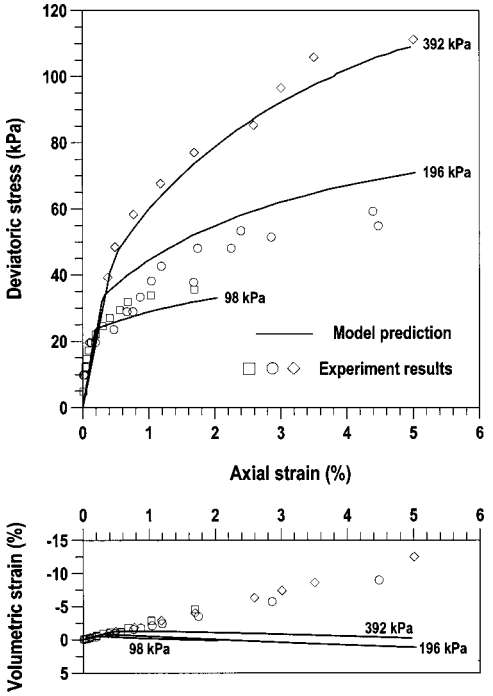

Fig. 7. Reduced triaxial compression test results and model predictions. Residual red clay (3.5 m deep).

ratory tests for the soil collected at depth of 3.5 m. Similar comparisons were obtained for the soil collected at depth of 6.5 m. The agreement between predicted and experimental results is reasonably good for the deviatoric stress curves. However, for the volumetric strain the agreement is good only for stress ratios (SRs) greater than 1.7 (i.e., for stress levels less than approximately 60% of the stress level at failure). For SRs between 1.7 and 1.0 (failure condition), Lade's model predicted a dilatant behavior, which contradicts experimental observations.

Fig. 8 compares the behavior of residual variegated clay following a RTC stress path as predicted by Lade's model and as obtained from the laboratory tests. The agreement between predicted and experimental results is good for both deviatoric stress

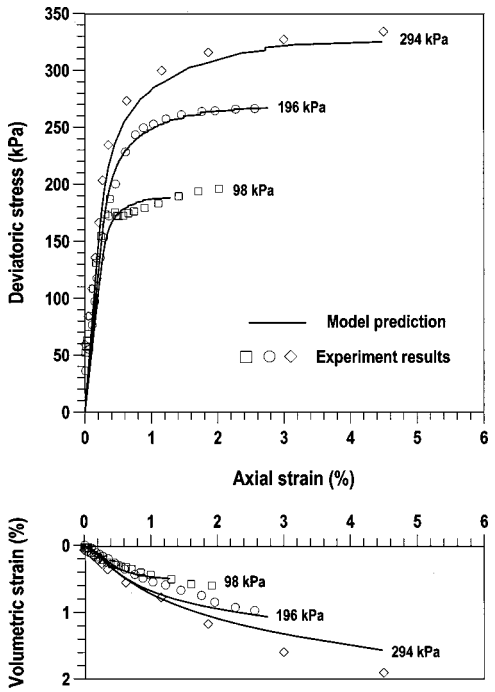

Fig. 6. Conventional triaxial compression test results and model predictions. Residual variegated clay layer.

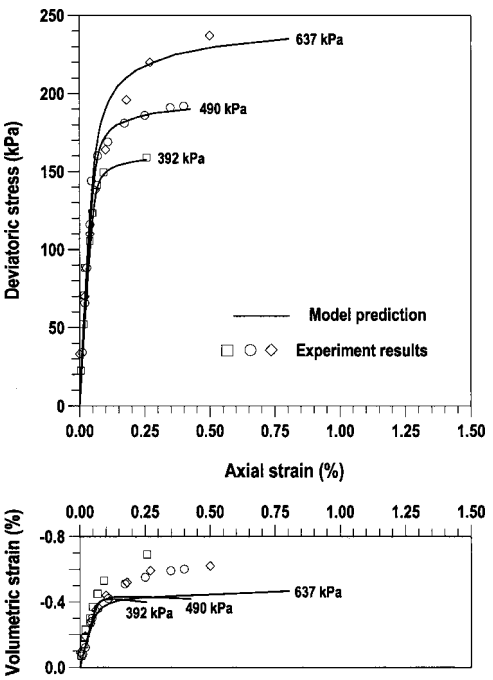

Fig. 8. Reduced triaxial compression test results and model predictions. Residual variegated clay layer.

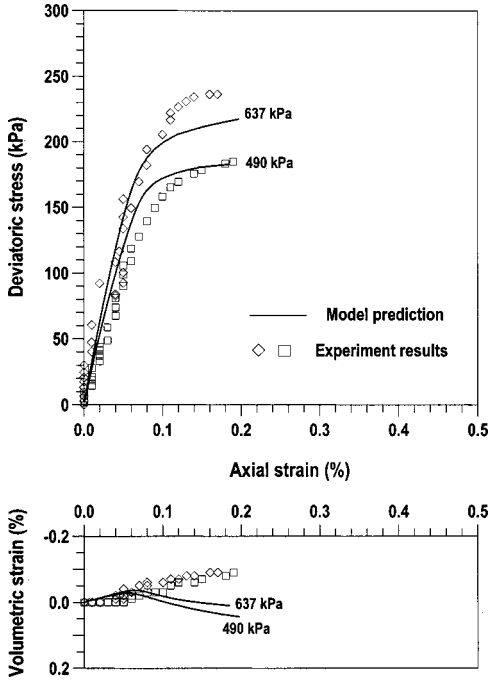

Fig. 9. Reduced triaxial extension test results and model predictions. Residual variegated clay layer.

and volumetric strain results corresponding to SRs above approximately 1.2 (i.e., stress levels less than approximately 80% of the stress level at failure).

RTE is a stress path typical of the soil mass located at the bottom of excavations. Consequently, because of the location of the residual variegated clay layer (see Fig. 2), a RTE stress path is relevant for this material and was included as part of the laboratory testing program. Fig. 9 compares the behavior of residual variegated clay under this stress path as predicted by Lade's model and as obtained from the laboratory tests. The agreement between predicted and experimental results is fairly good, particularly for SRs greater than approximately 1.2 (i.e., below 80% of the stress level at failure).

The differences observed in the volumetric behavior predicted by the model will not significantly effect the results of the numerical simulation because, as will be shown later, the SR is small (e.g., smaller than two) only in a very small region close to the tunnel floor. The residual variegated clay located at this region is much stiffer than the residual red clay and does not significantly influence the ground movements induced by the tunnel excavation. Moreover, the stress levels induced by the tunnel excavation in the entire residual red clay layer were far from failure (i.e., stress levels at which the model response was fairly good).

Numerical Simulation of Tunneling Process

The finite element simulation of a tunnel excavation through soils should ideally be performed using a 3D analysis. However, due to high computational costs, nonlinear 3D analyses are typically not performed for most projects. Thus, a methodology that approximately accounts for 3D effects using a 2D analysis was used for the numerical evaluation of the Paraíso tunnel.

The 2D finite element simulation of the Paraíso tunnel was performed in four stages:

1. *Determination of initial in situ stresses* [Fig. 10(a)]: The initial stresses within the soil mass are established assuming that they are characterized by a K_0 condition. The nodal forces equivalent to the in situ stresses along the perimeter of the excavation ($-P_0$) are calculated. These equivalent nodal forces are used in subsequent stages of the simulation to estimate the imposed forces on the excavation perimeter.
2. *Simulation of stress relief before excavation of the tunnel section* [Fig. 10(b)]: The stress state induced within the soil mass before the heading of the excavation reaches the section under evaluation is simulated. This is performed by applying a fraction α of the equivalent nodal forces P_0 calculated along the perimeter of the future tunnel excavation. The coefficient α is estimated by evaluating the magnitude αP_0 of nodal forces necessary to induce the surface settlement at the instrumented section immediately before the heading of the excavation reaches this section.
3. *Simulation of stress relief during excavation of the tunnel section* [Fig. 10(c)]: The stress state in the soil mass when the head of the excavation reaches the section under evaluation, but before the liner is installed, is determined. This is done by excavating the soil elements and by a trial-and-error procedure that determines the fraction ζ of the equivalent nodal forces P_0 which will induce incipient failure of the tunnel. Incipient failure is defined numerically when no convergence can be achieved using the incremental-iterative solution of the nonlinear problem. Subsequently, nodal forces βP_0, where β is equal to ζ divided by a reduction (safety) factor F, are applied along the perimeter of the tunnel.
4. *Simulation of stress relief after liner installation* [Fig. 10(d)]: The stress state induced in the soil mass following installation of the liner is determined. The material properties of the soil elements surrounding the tunnel are changed to those of the shotcrete liner. The remaining fraction η of the equivalent nodal forces P_0, where $\eta=1-(\alpha+\beta)$, are applied in this stage.

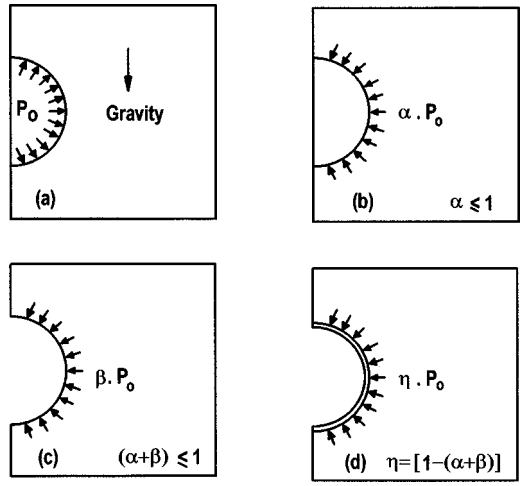

Fig. 10. Two-dimensional simulation of tunneling process

Numerical Simulation of Paraiso Tunnel

The 2D plane strain analysis of the Paraíso Tunnel was performed using the finite element code *ANLOG*, which is a multipurpose, nonlinear finite element program developed for analysis of geotechnical projects (Zornberg and Azevedo 1990). Eight-node isoparametric plane strain elements are used to model soil, and three-

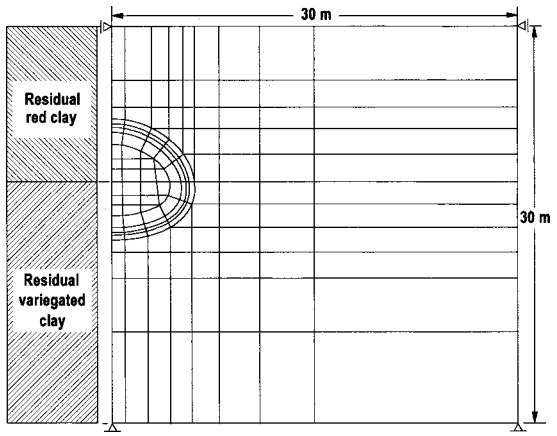

Fig. 11. Finite element mesh used in numerical simulation

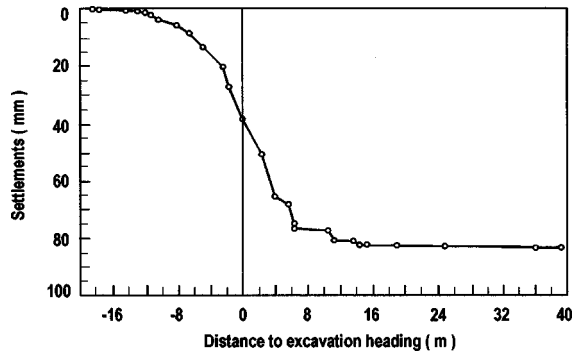

Fig. 12. Variation of surface settlement at instrumented section with distance to excavation heading

node bar elements are used to simulate struts and anchors. One of the several models implemented in the program is the nonassociated elastoplastic model developed by Lade (1977, 1979).

In order to facilitate simulations involving sequential analyses, a macrocommand feature was implemented in the program. This feature uses a set of compact and independent subprograms, each one designed to compute one or just a few basic steps in the finite element simulation process. The use of macrocommands is particularly useful to simulate the sequential construction of geotechnical structures such as tunnels, excavations and embankments.

Numerical simulation of excavations is performed by releasing equivalent nodal forces defined by the in situ soil stresses existing along the excavation perimeter before construction. Calculation of the equivalent nodal forces is performed using either the procedure proposed by Clough and Mana (1976) or the procedure proposed by Brown and Booker (1985). Elements and nodes within the perimeter of the excavation are removed from the mesh during the numerical simulation and the nodes remaining in the mesh are automatically renumbered before proceeding to the subsequent stages of the finite element analysis. An updated version of the *ANLOG* code incorporates fully coupled (deformation-pore pressure dissipation) analyses (Nogueira 1998).

As the section of the Paraíso tunnel and the geotechnical profile are symmetric, only half of the tunnel cross section was simulated. The finite element mesh and the soil profile used in the analyses are shown in Fig. 11. The mesh consisted of 154 elements and 503 nodal points.

The constitutive behavior of the residual clays was modeled using Lade's elastoplastic model with the parameters listed in Table 2. The constitutive parameters for the linear system are also needed for the analysis (Walter 1997). Because of lack of experimental data regarding stiffness of shotcrete liner systems as well as regarding the time dependency of the liner properties, a parametric study was performed using a linear-elastic and time independent model to simulate the liner behavior. The vertical displacements calculated at the crown of the tunnel for liner modulus values of 5, 10, and 20 GPa were 118, 116, and 114 mm, respectively. These results suggest that the tunnel response, for the range of modulus values considered in this evaluation, is not very sensitive to the selected liner modulus. Based on the results of this parametric assessment, a liner modulus of 10 GPa was selected for the final evaluation of the Paraíso tunnel.

The magnitude of excavation-induced displacements is highly sensitive to the state of stress within the soil mass prior to the excavation. An in situ stress state defined by a K_0 condition was assumed before tunnel construction. As mentioned before, K_0 values obtained in the laboratory were 0.58 for the residual red clay layers (3.5 and 6.5 m) and 0.84 for the residual variegated clay layers (9.5 and 12.5 m). However, considering the difficulties of accurately defining K_0 from undisturbed soil samples of overconsolidated soils, a sensitivity analysis was also performed in this case. This sensitivity study focused only on the K_0 values for the residual red clay layers, as most of the displacements are in these layers. The best agreement between field and numerical results was obtained for a K_0 value of 0.40 for the residual red clay layers. Therefore, the finite element analysis was finally performed using K_0 values of 0.40 and 0.84 for the residual red clay and residual variegated clay layers, respectively.

The final simulation was performed using the four stages described previously to represent the tunnel advancement (Fig. 10). For the stress relief before excavation of the tunnel section (Stage b), the surface settlement required to determine coefficient α should be estimated using previous field observations or, in situations were these observations are not available, by approximated analyses of the longitudinal tunneling advance (Hanafy and Emery 1982; Pierau 1982). The in situ surface settlement measured at the Paraíso tunnel centerline when the excavation heading reached the instrumented section was 38.2 mm, which corresponds to 46% of the total settlement (Fig. 12). A coefficient α of 0.60 was obtained, which defines the magnitude of nodal forces required to numerically obtain this measured settlement.

The fraction of the equivalent nodal forces that induces the incipient failure of the tunneling simulation process (Stage c) was estimated as $0.29\,P_0$. The selected value for the β coefficient was determined using a reduction factor $F=1.4$. Consequently, β was 0.21 ($\beta=0.29/F$) to simulate the stress relief after excavation of the tunnel section. The reduction factor F can be correlated with the ''standup time,'' which is the time for tunnel excavations to remain open before the roof begins to fail. If the standup time is short, F will be close to one as the tunnel will be brought to the verge of failure. For increasing values of standup times, F will be progressively larger than one.

Five load increments and an iterative procedure using the Newton–Raphson method were used in each stage of the excavation simulation. Stress and displacement fields were obtained in the soil elements for each stage of the analysis.

Fig. 13 shows the results of total (final) surface settlements profile induced at the instrumented section by the tunnel excavation. The field data in Fig. 13 is compared to the profiles obtained from the numerical analysis and from available empirical meth-

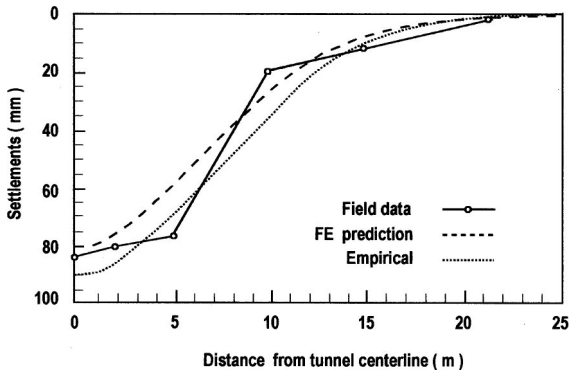

Fig. 13. Comparisons of final surface settlement profiles at instrumented section

ods. The subsidence δ_v obtained empirically was expressed as a Gaussian function of the distance y to the tunnel centerline defined by (e.g., Peck 1969):

$$\delta_v(y) = \delta_m \exp(-y^2/2i^2) \tag{11}$$

where δ_m = the maximum settlement above the tunnel crown and i = a parameter for which different expressions have been proposed in the literature. One such expression (New and O'Reilly 1991) is obtained as follows:

$$i = KH \tag{12}$$

where H = the distance from the tunnel axis to the surface and K = a parameter depending on the soil type ($K = 0.6$ for clays).

The short-term volume V_s of the subsidence bowl (for unit tunnel length) can be obtained from Eq. (11) as:

$$V_s = 2.5i\delta_m \tag{13}$$

In cohesive soils, this volume is equal to the "lost ground" volume, V_L. "Lost ground" volume is the volume of soil initially outside the future lining region, which is removed during excavation. A ratio of V_L/V_T equal to 2% is typical for soft soils (Shirlaw and Doran 1988), where V_T = excavated volume per unit tunnel length. This allows Eq. (13) to be solved for the maximum settlement δ_m as:

$$\delta_m = V_T/(125i) \tag{14}$$

In the case under consideration, $V_T = 82\ \text{m}^3/\text{m}$, $K = 0.6$, $H = 12$ m, so that Eqs. (12) and (14) lead to $i = KH = 7.2$ m and $\delta_m = 0.09$ m.

These results allow the settlement profile to be calculated by means of Eq. (11), as shown in Fig. 13. It can be seen that the empirical prediction is in good agreement with the measured and finite element displacements.

Significant assumptions were made to obtain the empirical relationship for the case of residual clay soils. Nonetheless, the good agreement between empirical results, for which significant experience has been accumulated over the years, and numerical results is encouraging.

When compared with semi-empirical analyses, the proposed numerical simulation is certainly more laborious and expensive. However, in addition to subsidence curves that can be obtained semi-empirically, the numerical analysis can provide the entire field of (vertical and horizontal) displacements, the stress state and the stress level within the soil mass at any stage of the tunnel excavation, as well as the stresses and displacements of the lining support system.

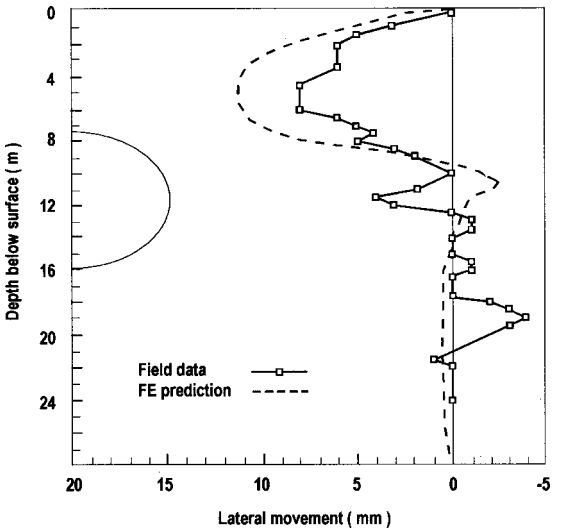

Fig. 14. Comparisons of final horizonal displacement profiles at instrumented section

Fig. 14 shows a comparison between the total (final) horizontal displacements monitored at the instrumented section by the inclinometer and the values predicted by the finite element analysis. Also in this case, a good comparison is observed between field and numerical results.

Fig. 15 shows contours of the mobilized stress ratio [Eq. (9)] obtained within the soil mass adjacent to the tunnel after excavation was completed. The numerical simulation shows no development of a generalized failure mechanism. Indeed, the results indicate that the shear strength of the soil is fully mobilized (i.e., SR close to one) in a small and localized area towards the base of the tunnel. The residual variegated clay in this location is mainly subjected to RTE stress paths. As discussed previously, the constitutive model showed good agreement with the experimental data up to approximately 80% of the stress level at failure. Consequently, the volumetric behavior obtained by the numerical analysis is not strictly correct in this area. However, the errors in this region did not influence the overall good performance of the numerical results because the residual variegated clay is much stiffer than the residual red clay, the region is comparatively

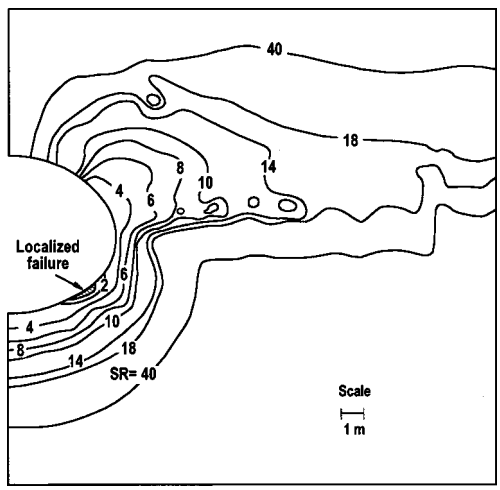

Fig. 15. Stress ratio isocurves defining mobilized shear strength

small, and most of the soil mass surrounding the excavation has a SR much greater than two, a condition for which the model representation of the volumetric behavior was good.

Summary and Conclusions

The ability of a finite element numerical simulation to reproduce the behavior of a shallow tunnel in residual soils was evaluated by conducting a back analysis of the Paraíso tunnel performance. The stress–strain–strength behavior of the residual soils was represented by a nonassociated elastoplastic model, which was calibrated using the results of a comprehensive laboratory testing program. Both loading and unloading stress paths, typical of excavation projects, were conducted as part of the testing program using undisturbed, unsaturated soil samples. A stress transfer method was proposed in order to simulate, using a 2D finite element analysis, the 3D characteristics of the tunnel excavation process.

Comparisons between the laboratory test results and the elastoplastic model predictions demonstrated the ability of the model to represent the deviatoric stress–axial–strain curves of the residual soils under different stress paths. For some stress paths typical of excavations, the volumetric strain–axial–strain curves predicted by the model did not show good results for stress levels close to the failure condition. Although limited by this observation, the model reproduced the experimental laboratory results reasonably well. This is particularly relevant since there is little experience in the technical literature regarding the use of elastoplastic models for undisturbed residual soils, which are typically unsaturated and slightly overconsolidated.

The procedure proposed to simulate the 3D tunnel advance using a 2D finite element simulation involves the determination of two parameters, α and β. The surface settlement required to obtain parameter α can be evaluated by using previous field observations or, if these are not available, by 2D numerical simulations of the longitudinal tunneling advance process. Parameter β is obtained by determining the loading required to numerically induce failure (no convergence in the numerical solution) and by subsequently reducing this loading by a factor of safety.

The results obtained from the numerical simulation showed good general agreement with the in situ monitored displacements. Most of the ground movements induced by the tunnel excavation occurred within the residual red clay layer, the stiffness of which is significantly smaller than that of the residual variegated clay layer. The stress levels induced by the tunnel excavation within the residual red clay layer were far from failure and, in these circumstances, the model response was fairly good. Although a small localized failure area occurred towards the bottom of the tunnel, its presence does not influence the overall good results obtained from the numerical simulation.

Overall, the results of this investigation showed the ability of a 2D elastoplastic finite element analysis to evaluate the deformations induced in residual soils by shallow tunnel excavations. Key elements in such simulations are: (1) the use of advanced constitutive models, calibrated using the results from careful laboratory testing programs, (2) the use a finite element code capable of accommodating nuances in the tunnel construction stages, and (3) the determination of coefficients proposed in this study to simulate the tunneling process.

Acknowledgment

The writers are indebted to Dr. Fulvio Tonon for his review of the paper and helpful suggestions.

References

Alonso, E. E., Gens, A., and Josa, A. (1990). ''A constitutive model for partially saturated soils.'' *Geotechnique,* 40(3), 405–430.

Augarde, C. E., Burd, H. J., and Houlsby, G. T. (1995). ''A three-dimensional finite element model of tunneling.'' *Proc., 5th Symposium on Numerical Models in Geomechanics*, 1, 457–462.

Bernat, S., and Cambou, B. (1995). ''Modeling of tunnel excavation in soft soil.'' *Proc., 5th Symposium on Numerical Models in Geomechanics*, 1, 471–476.

Brown, P. T., and Booker, J. R. (1985). ''Finite element analysis of excavations.'' *Comp. Geotechn.,* 1, 207–220.

Clough, G. W., and Mana, A. I. (1976). ''Lessons in finite element analyses of temporary excavations in soft clay.'' *Proc., 2nd Int. Conf. on Numerical Methods in Geomechanics*, 496–510.

Eisenstein, Z., and Sorensen, K. L. (1986). ''Tunneling for the south LRT extension in Edmonton: Alberta.'' *Canadian Tunneling,* 19–30.

Hanafy, E. A., and Emery, J. J. (1982). ''Three-dimensional simulation of tunnel excavation in squeezing ground.'' *Proc., 4th Int. Conf. on Numerical Methods in Geomechanics*, 3, 1203–1209.

Kupper, A. A. G., Costa Filho, L. M., and Antunes, F. S. (1985). ''Geotechnical characterization of the São Paulo red clay.'' *Proc., 1st Int. Conf. on Geomechanics in Tropical Lateritic and Saprolitic Soils*, Vol. 1, 117–129.

Lade, P. V. (1977). ''Elastoplastic stress-strain theory for cohesionless soil with curved yield surfaces.'' *Int. J. Solids Struct.,* 13, 1019–1035.

Lade, P. V. (1979). ''Stress-strain theory for normally consolidated clay.'' *Proc., 3rd Int. Conf. on Numerical Methods in Geomechanics*, Vol. 4, 1325–1337.

Leroueil, S. (1997). ''Critical state soil mechanics and the behavior of real soils.'' *Proc., Int. Symposium on Recent Developments in Soil and Pavement Mechanics*, 41–80.

Malato, P., Torrado da Silva, J., Marques, J., and Almeida e Sousa, J. (1998) ''Lisbon metro—Behavior of a shallow tunnel in stiff clay.'' *Proc., World Tunnel Congress 1998 on Tunnels and Metropolises*, Vol. 2, 1169–1174.

Massad, F., Samara, V., and Barros, J. M. C. (1985). ''Engineering properties of two layers of lateritic soils from São Paulo city, Brazil.'' *Proc., 1st Int. Conf. on Geomechanics in Tropical Lateritic and Saprolitic Soils*, Vol. 1, 331–343.

Negro, A. (1998). ''General report: Design criteria for tunnels in metropolises.'' *Proc., World Tunnel Congress 1998 on Tunnels and Metropolises*, Vol. 1, 201–214.

Negro, A., and Eisenstein, Z. (1991). ''Shallow tunnels in soft ground: State-of-the-art report.'' *Proc., 9th Pan. Conf. on Soil Mechanics and Foundations Engineering*, in Post Conference Volume, 23–42.

New, B. M., and O'Reilly, M. P. (1991). ''Tunneling induced ground movements: Predicting their magnitude and effects.'' *Proc., 4th Int. Conf. on Ground Movements and Structures,* 671–697.

Ng, R. M. C., and Lo, K. Y. (1985). ''The measurements of soil parameter relevant to tunneling in clays.'' *Can. Geotech. J.*, 22, 375–395.

Nogueira, C. (1998). ''Non-linear analysis of excavations and embankments.'' (in Portuguese) PhD thesis, PUC-Rio, Brazil.

Panet, M., and Guenot, A. (1982). ''Analysis of convergence behind the face of a tunnel.'' *Tunneling 1982*, Institute of Mining and Metallurgy, 197–204.

Parreira, A. B. (1991). ''Analysis of shallow tunnels in soil. The Mineiro-Paraíso tunnel at Paulista Avenue in São Paulo City.'' (in Portuguese) PhD thesis, PUC-Rio, Brazil.

Peck, R. B. (1969). ''Deep excavations and tunneling in soft ground.'' *Proc., 7th Int. Conf. on Soil Mechanics and Foundations in Engineering*, 225–290.

Pierau, B. (1982). ''Tunnel design with respect to the three-dimensional state of stress and displacements around the temporary face.'' *Proc., 4th Int. Conf. on Numerical Methods in Geomechanics*, Vol. 3, 1221–1231.

Schikora, K., and Ostermeier, B. (1988). ''Two-dimensional calculation model in tunneling-verification by measurement results and by spatial calculation.'' *Proc., 6th Int. Conf. on Numerical Methods in Geomechanics*, Vol. 3, 1499–1503.

Shirlaw, J. N., and Doran, S. (1988). ''Ground movements and settlements caused by tunneling for the singapore mass rapid transit System.'' *Tunneling*, 88, 295–314.

Targas, D. N., Junior, M. D., and Oliveira, R. A. (1998). ''Design and construction of the enlargement of a tunnel section of unusual dimension.'' *Proc., World Tunnel Congress 1998 on Tunnels and Metropolises*, Vol. 2, 993–1000.

Walter, H. (1997). ''Application of a new shotcrete model in a 3-D-FE-analyis of a tunnel.'' *Proc., 6th Int. Symposium on Numerical Models in Geomechanics*, 455–460.

West, T. R. (1995). *Geology applied to engineering*, Prentice–Hall,Englewood Cliffs, N.J.

Whittle, A. J., Hashash, Y. M. A., and Whitman, R. V. (1993). ''Analysis of deep excavation in Boston.'' *J. Geotech. Eng.*, 119(1), 69–90.

Zornberg, J. G., and Azevedo, R. F. (1990). *ANLOG*: Nonlinear analysis of geotechnical projects-user's guide (in Portuguese), *Internal Rep. No. RI 03/90*, Civil Engineering. Dept., PUC-Rio, Brazil.

Zornberg, J. G., and Azevedo, R. F (1998). ''Numerical prediction of the behavior of an excavation in residual soils.'' *Proc., World Tunnel Congress 1998 on Tunnels and Metropolises*, Vol. 1, 417–422.